Received: 15 March 2022 | Revised: 18 July 2022 | Accepted: 13 October 2022

DOI: 10.1111/clr.14014

CLINICAL ORAL IMPLANTS RESEARCH WILEY

ORIGINAL ARTICLE

# Antimicrobial efficiency and cytocompatibility of different decontamination methods on titanium and zirconium surfaces

Jamal M. Stein[1,2] | Georg Conrads[3] | Mohamed M. H. Abdelbary[3] | Sareh Said Yekta-Michael[4] | Patricia Buttler[1] | Joanna Glock[1] | Gelareh Sadvandi[1] | Robert Kaufmann[5] | Christian Apel[6]

[1]Operative Dentistry, Periodontology and Preventive Dentistry, University Hospital (RWTH), Aachen, Germany

[2]Private Practice, Aachen, Germany

[3]Division of Oral Microbiology and Immunology, Department of Operative Dentistry, Periodontology and Preventive Dentistry, Rheinisch-Westfälische Technische Hochschule (RWTH) Aachen University Hospital, Aachen, Germany

[4]Department of Orthodontics, RWTH Aachen University Hospital, Aachen, Germany

[5]DWI - Leibnitz-Institut für Interaktive Materialien, Aachen, Germany

[6]Department of Biohybrid & Medical Textiles (BioTex), Institute of Applied Medical Engineering, RWTH Aachen University & Hospital, Germany

**Correspondence**
Jamal M. Stein, Department of Operative Dentistry, Periodontology and Preventive Dentistry, University Hospital Aachen (RWTH), Pauwelsstrasse 30, D-52074 Aachen, Germany.
Email: jstein@ukaachen.de

**Funding information**
Oral Reconstruction Foundation, Grant/Award Number: ORF11802

## Abstract

**Objectives:** The purpose of this study was to investigate the efficiency of different implant-decontamination methods regarding biofilm modification and potential cytotoxic effects. Therefore, the amount of biofilm reduction, cytocompatibility, and elementary surface alterations were evaluated after decontamination of titanium and zirconium surfaces.

**Material and Methods:** Titanium and zirconium disks were contaminated with a newly developed high-adherence biofilm consisting of six microbial species. Decontaminations were performed using titanium curette, stainless steel ultrasonic scaler (US), glycine (GPAP) and erythritol (EPAP) powder air-polishing, Er:YAG laser, 1% chlorhexidine (CHX), 10% povidone-iodine (PVI), 14% doxycycline (doxy), and 0.95% NaOCl solution. Microbiologic analysis was done using real-time qPCR. For assessment of cytocompatibility, a multiplex assay for the detection of cytotoxicity, viability, and apoptosis on human gingival fibroblasts was performed. X-ray photoelectron spectroscopy (XPS) was used to evaluate chemical alterations on implant surfaces.

**Results:** Compared with untreated control disks, only GPAP, EPAP, US, and Er:YAG laser significantly reduced rRNA counts (activity) on titanium and zirconium ($p < .01$), whereas NaOCl decreased rRNA count on titanium ($p < .01$). Genome count (bacterial presence) was significantly reduced by GPAP, EPAP, and US on zirconium only ($p < .05$). X-ray photoelectron spectroscopy analyses revealed relevant re-exposure of implant surface elements after GPAP, EPAP, and US treatment on both materials, however, not after Er:YAG laser application. Cytocompatibility was impaired by CHX, PVI, doxy, and NaOCl. CHX and PVI resulted in the lowest viability and doxy in the highest apoptosis.

**Conclusions:** Within the limits of this in vitro study, air-polishing methods and ultrasonic device resulted in effective biofilm inactivation with surface re-exposure and favorable cytocompatibility on titanium and zirconium. Chemical agents, when applied on implant surfaces, may cause potential cytotoxic effects.

KEYWORDS
biofilm, decontamination, peri-implantitis, titanium, zirconium

## 1 | INTRODUCTION

Peri-implant mucositis and peri-implantitis are the most frequent biological complications of dental implants that are primarily caused by a non-specific polymicrobial biofilm (Daubert & Weinstein, 2019; Renvert et al., 2018). Prevention and therapy of peri-implant diseases focus on removal or disruption of the peri-implant biofilm in order to re-establish a biocompatible implant surface. However, the structure and the wide spectrum of microorganisms in this biofilm (Charalampakis & Belibasakis, 2015; Padial-Molina et al., 2016; Rakic et al., 2016) together with the limited access to contaminated implant surfaces (Sanz-Martín et al., 2021; Steiger-Ronay et al., 2017) represent a challenge for every therapy. Non-surgical treatment has been shown to yield favorable results for peri-implant mucositis (Heitz-Mayfield & Salvi, 2018; Schwarz et al., 2015). By contrast, for peri-implantitis, mechanical non-surgical therapy alone was reported to be not efficient and inferior to surgical approaches with regenerative or resective measures (Chan et al., 2014; Schwarz et al., 2015) because mechanical instrumentation using curettes or ultrasonic devices is complicated by the design of macro- and microthreads of the implants (Sanz-Martín et al., 2021). To compensate this problem, alternative decontamination methods such as air-polishing, laser-assisted therapies, and the application of different antimicrobial agents (e.g., chlorhexidine) or local antibiotics (e.g., doxycycline) have been recommended (Faggion et al., 2014; Schwarz et al., 2015).

Several in vitro studies have investigated the efficiency of biofilm removal on titanium implant surfaces. While Er:YAG laser (AlMoharib et al., 2021; Eick et al., 2017) and air-abrasive devices (Keim et al., 2019; Leung et al., 2022; Tuchscheerer et al., 2021) proved to be effective, curettes and sonic / ultrasonic devices cleaned the surfaces poorly (AlMoharib et al., 2021; Keim et al., 2019; Sahrmann et al., 2015). Chemotherapeutic agents such as chlorhexidine, phosphoric acid (Dostie et al., 2017) citric acid (Cordeiro et al., 2021; Kotsakis et al., 2016), and NaOCl-EDTA (Kotsakis et al., 2016) demonstrated modest and favorable antimicrobial effects on biofilms on titanium surfaces. Thereby, a few of the aforementioned studies used multispecies biofilm models (Cordeiro et al., 2021; Eick et al., 2017) or plaque samples from subjects (AlMoharib et al., 2021; Dostie et al., 2017; Wheelis et al., 2016). Furthermore, there is growing but still limited evidence about cytocompatibility of decontamination methods (Kotsakis et al., 2016; Ungvári et al., 2010; Wheelis et al., 2016). Modification of implant surfaces, such as dissolution of titanium components (Wheelis et al., 2016) and cytotoxic effects on fibroblasts or osteoblasts (Kotsakis et al., 2016), may impair re-osseointegration or induce inflammatory effects.

Moreover, all previous studies on the efficiency of decontamination were performed on titanium materials, whereas for zirconium, equivalent data are not available yet. There is growing evidence that zirconium implants might be a promising alternative due to their favorable biocompatibility and esthetic benefits (Comisso et al., 2021). However, since peri-implant diseases may also affect zirconium implants (Becker et al., 2017; Fretwurst et al., 2021), information about appropriate decontamination measures for these surfaces is needed. Therefore, the aim of the present study was to investigate the efficiency of biofilm reduction and cytocompatibility of different implant-decontamination methods on both titanium and zirconium surfaces.

## 2 | MATERIALS AND METHODS

Titanium and zirconium disks (15 mm diameter, 1 mm thickness) were used for all decontamination tests with (microbial and XPS analysis) and without (cell culture analyses) prior biofilm contamination. Titanium material fulfilled the requirements for grade 4 commercially pure titanium (standards ISO 5832-2 and ASTM f67). The surface was corundum blasted and acid etched with a roughness average (RA) value of 1.3 µm. Zirconium disks were composed of yttria-stabilized zirconium and had a RA value of 1.1 µm. All disks were autoclaved before their use. After autoclavation, all disks were stored in separate wells of a 12-well microtiter plate avoiding contamination and disk–disk contact. Although oxygen was present near the surface of all disks in compound form ($TiO_2$; $ZrO_2$), for simplification, the terms titanium and zirconium shall be used throughout the following text.

### 2.1 | High-adherence biofilm model

To develop a peri-implantitis-biofilm model for testing implant-decontamination conditions under harsh conditions, a new approach was applied combining microbial species with the most aggregation (*Aggregatibacter actinomycetemcomitans*, *Fusobacterium nucleatum*), adhesive (*Streptococcus sanguinis/oralis*), and net-forming (mycelia by *Candida albicans*, pseudo-mycelia by *Actinomyces oris*) potential (Chen et al., 2022; D'Ercole et al., 2020; Hauser-Gerspach et al., 2007). The primary goal was to create a manageable, reproducible, and robust, water-insoluble biofilm to challenge any implant-decontamination method to the most. As natural, fresh isolates have more surface antigens for mediating adherence/aggregation than laboratory strains, the strains were re-activated by adding sterile-filtered saliva and horse blood.

### 2.2 | Contamination protocol

The test species from our stocks (*Aggregatibacter actinomycetemcomitans* ATCC 33384 T, *Actinomyces oris* OMI 235, *Candida albicans* OMI 286, *Fusobacterium nucleatum* ATCC 25586 T, *Streptococcus sanguinis* OMI 332, and *Streptococcus oralis* ATCC 35037 T) were primarily

grown at 37°C in an appropriate medium at appropriate conditions (see Table 1). After sufficient growth (24-72 h), five colonies of each test species were separately and homogeneously suspended in 5-ml saline solution (0.9%). The exact cell concentrations were determined by plating an aliquot. A volume between 100 and 200 µl of theses suspensions with the CFU numbers given in Table 1 was used for inoculating the disks (placed in 12-well microtiter wells and overlaid with 1 ml Mueller–Hinton Bouillon as well as 40 µl 50% sucrose solution). On Day 1, firstly, a volume of 70-µl sterile-filtered saliva and 70-µl horse blood was added and—as the first two species—*C. albicans* and *A. oris* were inoculated, allowing formation of both a wide-meshed and closed-meshed net. Microtiter plates were incubated anaerobically by using the BD GasPak EZ anaerobe gas generation pouch system (Thermo Fisher Scientific, Dreieich, Germany) for 7 days. On Day 2, slow-growing *A. actinomycetemcomitans* and *F. nucleatum* were added. Both species form aggregates and are known to co-adhere with other bacteria. Finally, on Day 3, the two fast-growing streptococcal species were added and the—in total—six-species biofilm grown for an additional 4 days (Figure S1a). At Day 7, the appropriateness of biofilm was ensured by live-/dead- and Gram staining (Figure S1b,c), and the culture terminated. The biofilm-covered disks were removed, cleaned, and dried only on the (almost biofilm-free) underside by the aid of an absorbent paper and ethanol, and transferred and fixed—with a little silicon on the underside—in the lid of a 12-well plate to ease handling later (Figure S1d). Disks were incubated for around 10 min. at 37°C until excess water was removed (Figure S1e). The lid with fixed disks was closed with the plate (upside down as the plate is usually closed with its lid), and the stack of plates (Figure S1f) was frozen at −80°C until further procedures [staining for quality control, decontamination (example given in Figure S1g), X-ray photoelectron spectroscopy analysis, see below].

**TABLE 1** Microbial strains, growth medium, conditions, and inoculum used in this study

| Species and strain | Medium and growth condition | CFU[$] number for inoculum |
|---|---|---|
| *Aggregatibacter actinomycetemcomitans* ATCC 33384[T] | BHI, capnophilic[§], 72 h | $2.34 \times 10^4$ |
| *Actinomyces oris* OMI 235 | MH, capnophilic[§], 72 h | $1.56 \times 10^4$ |
| *Candida albicans* OMI 286 | Saboraud, capnophilic[§], 24 h | $1.08 \times 10^4$ |
| *Fusobacterium nucleatum* ATCC 25586[T] | BHI, anaerobic*, 24 h | $2.10 \times 10^4$ |
| *Streptococcus oralis* ATCC 35037[T] | MH, capnophilic[§], 24 h | $1.05 \times 10^4$ |
| *Streptococcus sanguinis* OMI 332 | MH, capnophilic[§], 24 h | $1.06 \times 10^4$ |

*Note*: CFU[$] colony-forming units; [§]7%–8% $CO_2$; *by BD GasPak EZ anaerobe gas generation pouch system with indicator (order # 260683), Becton–Dickinson.

Abbreviations: ATCC, American Type Culture Collection; BHI, Brain Heart Infusion broth; MH Mueller–Hinton broth; OMI, Oral Microbiology Immunology division (RWTH Aachen University, Germany).

## 2.3 | Decontamination protocol

Titanium and zirconium disks were decontaminated using the following procedures:

- Titanium curette (Langer curette IMPLG1/2 T, Hu-Friedy, Frankfurt, Germany)
- Stainless steel ultrasonic scaler [US (Piezon Master® with PS tip, EMS, Nyon, Switzerland)]
- Glycine powder air-polishing [GPAP (Air-Flow® with Air-Flow Perio®, EMS)]
- Erythritol powder air-polishing [EPAP (Air-Flow® with Air-Flow Plus®, EMS)]
- Er:YAG laser [100 mJ, 5 W, 50 Hz (LightTouch™, Yokneam, Israel)]
- 1% chlorhexidine (CHX) solution (1.0 g Chlorhexidingluconat 20%, Fagron GmbH & Co.KG, Barsbüttel, Germany, ad 100.0 g aqua injectabilia for 50 ml volume)
- 10% povidone-iodine (PVI) solution (Betaisodona®, Mundipharma, Frankfurt, Germany)
- 14% doxycycline (doxy) suspension (35 tablets DoxyHexal 200 mg, Hexal AG, Holzkirchen, Germany; ad 50.0 g aqua injectabilia for 50 ml volume)
- 0.95% NaOCl solution (AppliChem GmbH, Darmstadt, Germany)

All mechanical decontaminations (curette, US, GPAP, and EPAP) and Er:YAG laser irradiation were performed for 20 s under 0.9% NaCl cooling (except for curette) with equal instrumentation of the disk surfaces. Application of all chemotherapeutic agents (CHX, PVP, doxy, and NaOCl) was done using disposable syringes with sterile cannulas. Care was taken to ensure that disks were equally and completely covered by the agents without mechanical detachment of the biofilm. Exposure time was 2 min. Those disks that were used for microbiologic analyses were subsequently rinsed with six increments of 1 ml 0.9% NaCl according to the protocol of Dostie et al. (2017) in order to stop the antimicrobial activity. All other disks (used for cytocompatibility and surface analyses) were processed without subsequent rinsing. In total, experiments were performed on 153 titanium and 153 zirconium disks. For each decontamination per material, four disks were used for qualitative and quantitative microbiologic analysis, 12 for cell culture experiments (triplets for live/dead staining after 24 h, multiplex assays after 24 h and 48 h, and SEM microscopy after 24 h), and one for elementary analysis. Further, five positive (untreated biofilm contaminated) control disks per material were referred to microbiologic analysis (N = 4) and elementary analysis (N = 1), while eight negative (untreated sterile) control disks per material were used for cell culture tests.

All decontaminations were performed by two persons (JMS performed all mechanical procedures, SM conducted the laser and all chemical treatments). Prior to the study, all tests were exercised

by the same persons in order to get familiar with the procedures and to achieve an acceptable reproducibility of the performances. Treatments with curette, US, GPAP, EPAP, and Er:YAG laser were performed with controlled movements achieving maximum possible contact with the decontaminated disk surfaces, while all chemical agents were applied covering the whole disk surface.

## 2.4 | Microbiological analyses

A LIVE/DEAD Biofilm Kit (Filmtracer™ LIVE/DEAD™ Biofilm Viability Kit, Thermo Fisher Scientific, Dreieich, Germany) and epifluorescence microscopy (Microscope DMRX, Leica, Wetzlar, Germany) were used to visualize and semi-quantify the composition and viability of the high-adherence biofilm. Gram staining was performed to estimate gram-negative, gram-positive, and fungal cells ratio.

For quantitative analysis, the high-adherence biofilm was dispersed from test specimens with and without decontamination, the samples were centrifuged, and the pellets were washed with bidistilled water and frozen at −72°C until further processing. The pellets were resuspended in 200 µl bidistilled water. DNA and RNA were isolated using a DNA/RNA Extraction Kit (NucleoSpin RNA XS, Macherey-Nagel, Düren, Germany). For the initial lysis with lysozyme and mutanolysin (3-mg lysozyme, 100-U mutanolysin, in 200-µl Tris EDTA buffer, and 20 µl added to every sample), all samples were incubated at 37°C for 10 min and further isolation was performed according to the manual with elution volumes of 100 µl. Subsequently, 10 µl of the total RNA (1:10 dilution) was reversely transcribed into cDNA, using random hexamer primers (60 µM) with a cDNA Synthesis Kit (Transcriptor First Strand cDNA Synthesis Kit, Roche, Mannheim, Germany) according to the manual.

A qRT-PCR (QuantStudio 3, Thermo Fisher Scientific, Dreieich, Germany) was performed to measure (i) the bacterial genome numbers equivalent to cell numbers applying using universal, broad-spectrum bacteria-primers according to Nadkarni et al. (2002) and (ii) the bacterial activity represented by rRNA numbers, derived from cDNA quantification (Henne et al., 2016; Walther et al., 2021), in every treatment and control sample. DNA of a stock suspension (reference strain *Streptococcus oralis* ATCC 35037; $8.0x10^8$/ml) was serially diluted in tenfold steps with nuclease-free water and served as a standard curve. Every sample and control were measured in technical triplicates. Each well contained 20 µl of the reaction mix with the following components: 10-µl gene expression master mix (PowerUp™ SYBR™ Green Master Mix, Thermo Fisher Scientific, Dreieich, Germany), Nadkarni-Forward Primer (5′ TCCTACGGGAGGCAGCAGT 3′, 0.1 µl), Nadkarni-Reverse Primer (5′ GGACTACCAGGGTATCTAATCCTGTT 3′, 0.1 µl), 8-8 µl nuclease-free water, and 1-µl template. The concentration of both primers (TIB Molbiol, Berlin, Germany) was 100 µM. The qRT-PCR was performed with the following temperature profile: initial denaturation at 95°C (2 min); 40 cycles of 95°C (10 s), Ta = 60°C (10 s), 72°C (25 s); and final elongation at 72°C (10 min). As a negative control, nuclease-free water was added instead of the template.

In the case of the net-forming yeasts, a conventional colony-forming unit determination on Saboraud-Agar was performed. Since the number of yeast cells was below the number of bacteria by the magnitude of two logs, the *C. albicans* count could be neglected.

## 2.5 | Cell culture and cytocompatibility analyses

For cytocompatibility analyses, decontamination measures of all disks were performed as described above, however without prior contamination. Test samples were seeded with immortalized human gingival fibroblasts (hGF; 50.000 cells/sample; Immortalized Human Gingival Fibroblasts- hTERT, BioCat, Heidelberg, Germany) and cultured in 600 µl DMEM (Dulbecco's Modified Eagle Medium; Invitrogen AG, Carlsbad, USA) supplemented with 10% fetal bovine serum and 0.25 mg/mL gentamicin (both Invitrogen AG). Samples were incubated at 37°C under a supply of 5% $CO_2$ and removed after 24 or 48 h, respectively, for subsequent analyses. All measurements were performed in triplicates.

Pictures were performed to visualize effects of decontamination methods on hGF cell morphology, and surface characteristics of the two materials after decontamination treatments using a scanning electron microscope (ESEM XL30 FEG, FEI, Philips, Eindhoven, Netherlands) were performed for demonstration of morphological differences. The preparation of the samples was carried out by fixation with glutaraldehyde followed by critical point drying. Differences in viability were detected with live/dead staining. To this end, the samples were cultured in a 12-well plate containing 3 ml medium/well, rinsed with PBS after 24 and 48 h, respectively. After subsequent overlay with live/dead assay (LIVE/DEAD™ Cell Imaging Kit, Invitrogen AG), digital images of the stained disks were taken with an epifluorescence microscope (Microscope DMRX, Leica) within 1 h.

For the assessment of cytotoxicity, viability, and apoptosis in hGF cells on decontaminated samples, three independent fluorescence-based assays (CytoTox-ONE Homogeneous Membrane Integrity Assay, CellTiter-Blue Cell Viability Assay, and Apo-One Homogeneous Caspase-3/7 Assay, all Promega, Mannheim, Germany) were combined and adapted to analyze the three different parameters from one single sample, consecutively. The samples were measured on a multi-mode microplate reader (Spectramax ID3 with Software Soft Max Pro 7.1, Molecular Devices, San Jose, USA). For cytotoxicity, cell culture supernatant was mixed with CytoTox-ONE reagent after 24 and 48 h of cell growth, transferred to a 96-well plate, and measured at 540 Ex/580 Em after an incubation time of 10 min. For the subsequent measurements of viability, fresh medium was added to the samples together with CellTiter-Blue reagent incubated for 2 h and measured after transfer to a 96-well plate at 540 Ex/580 Em. To quantify caspase 3/7 activity, the Apo-ONE reagent was added to the remaining medium. After 18 h incubation, medium was transferred to a 96-well plate and measured at 485Ex/527Em.

### 2.6 | Analysis of elementary composition using X-ray photoelectron spectroscopy (XPS)

For evaluation of the chemical alterations of the surface of the decontaminated disks, the atomic composition was examined using XPS technology. In order to evaluate alterations on biofilm-covered and biofilm-free surfaces, all decontamination tests were performed on disks with and without prior contamination. Measurements were carried out in an XPS spectrometer (Ultra AxisTM spectrometer, Kratos Analytical, Manchester, UK). The excitation area of XPS was approximately $1 \times 1\,mm^2$. This area was chosen arbitrarily on the homogeneous surfaces in the central area of the disks. The samples were irradiated with monoenergetic Al $K_\alpha$1,2 radiation (1486.6 eV), and the spectra were taken at a power of 144 W (12 kV × 12 mA). The aliphatic carbon (C-C, C-H) at a binding energy of 285 eV (C 1 s photoline) was used to determine the charging. The spectral resolution—that is, the Full Width of Half Maximum (FWHM) of the Ester carbon from PET—was better than 0.68 eV for the elemental spectra. The elemental concentration is given in atom%, but it should be considered that this method can detect all elements except hydrogen and helium. The information depth was around 10 nm for polymers and 6 nm for metallic/inorganic materials.

### 2.7 | Statistical analyses

All results are presented as means or percentages with standard deviations (SD). Quantitative microbiologic and cell culture data were analyzed using a statistical software (GraphPad Prism, Version 9.0.0, San Diego, CA). Data were unpaired and not normally (not Gaussian) distributed. Therefore, the Kruskal–Wallis test was performed. For each material (titanium and zirconium), the mean rank of each treatment was compared with the mean rank of a negative control group (biofilm without treatment). For pairwise comparisons, Dunn's test including Bonferroni correction of the *p*-value was used. A probability of $p < .05$ was considered statistically significant.

## 3 | RESULTS

### 3.1 | Microbiologic results

Results of qualitative analysis of the high-adherence biofilm by live/dead and Gram staining are visualized in Figure S1b,c. The pseudomycelium of *Candida albicans* established the basic structure of the biofilm. *Actinomyces oris* formed bundles, cross-linking the yeast mycelium, while *Fusobacterium nucleatum served as* "bridging bacterium" mediating co-adhesion. *Streptococcus sanguinis*, *S. oralis*, and *Aggregatibacter actinomycetemcomitans* produced extracellular polysaccharides and/or served as filler.

Quantitative results of the decontaminations comprising reduction in the genome (or cell) and of the rRNA count, the latter an established parameter representing bacterial activity, are illustrated in Figure 1. While on titanium disks, all decontamination measures did not lead to significant differences, zirconium disks US, GPAP, and EPAP led to significantly higher reductions compared with the untreated control disk (Figure 1a). Considering bacterial activity, US, GPAP, EPAP, and Er:YAG laser led to significant reductions in rRNA counts both on titanium and zirconium surfaces, with even more pronounced reductions in GPAP, EPAP, and Er:YAG laser on zirconium disks. Besides, rRNA counts were significantly reduced by NaOCl on titanium surfaces, but not on zirconium (Figure 1b). All other measures did not show any significant deviations.

### 3.2 | Results of cytocompatibility analyses

Lactate dehydrogenase (LDH) secretion (measure for cytotoxicity), cell viability, and caspase 3/7 activity (measure for apoptosis) were determined for hGF seeded onto zirconium and titanium samples after different decontamination treatments. Results of this multivariate analysis are shown in Figure 2. Additional live/dead staining was performed to assess cytocompatibility qualitatively for all treatments and untreated controls. Figure 3 shows representative images of live/dead staining with viable (green) and dead (red) cells.

In general, the mechanical treatments (curette and US), both air-polishing abrasives and laser irradiation, showed the highest cell viability along with low cytotoxicity and apoptosis values (Figure 2). There was a reduced number of viable cells on zirconium samples after mechanical treatment and laser irradiation after 24 h of cultivation (Figure 2c,d). This effect, however, could not be observed after live/dead staining (Figure 3) or in SEM pictures (Figure 4). Among chemotherapeutic agents, CHX application induced a cytotoxic effect of 27% on zirconium and 41% on titanium samples (Figure 2a,b). This went along with a significantly reduced number of viable cells (Figure 2c,d) and high number of dead cells in the live/dead staining (Figure 3). There seemed to be a relief of this cytotoxic effect over time since the cells slightly recovered after 48 h (Figure 3a,b). NaOCl produced a minor cytotoxic effect on titanium, together with a reduced number of viable cells and a moderately increased signal for apoptosis. This effect could only be observed on titanium samples. On zirconium, by contrast, there was only a minimal increase in apoptosis. Interestingly, doxycycline treatment of the samples showed a slight cytotoxic effect but a significantly reduced number of viable cells and a pronounced apoptotic signal. It seems that doxycycline induced apoptosis in the cells, which even increased over time. PVI treatment led to low cytotoxicity, viability, and apoptosis signals, while live/dead staining resulted in nearly 100% dead cells 24 h after seeding onto PVI-treated titanium and zirconium samples (Figure 3).

### 3.3 | Results of elementary analysis (XPS)

Elementary composition of all decontaminated surfaces is shown in Tables 2 and 3. XPS analysis on titanium disks with prior biofilm

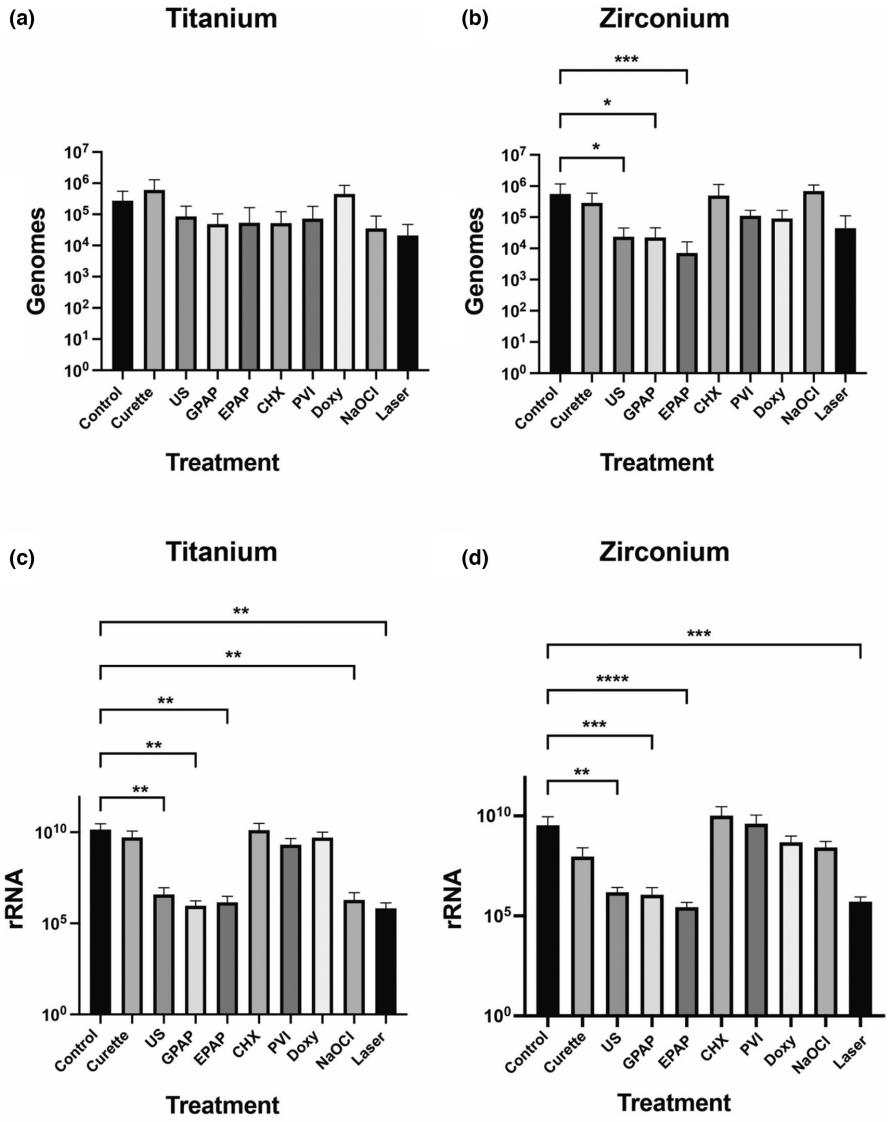


**FIGURE 1** Reduction in genome (cell) count (a on titanium and b on zirconium) and or rRNA count (representing bacterial activity, c on titanium, and d on zirconium) of high-adherence biofilm after decontamination compared with untreated control. $^{*}p < .05$, $^{**}p < .01$, $^{***}p < .001$, $^{****}p < .0001$. The Y-axis represents the log10 transformed bacterial genome/rRNA counts.

contamination showed a slightly increased percentage of Ti after decontamination with US, GPAP, and EPAP, while control disks and all other methods had no Ti signal (0%). Since XPS had a detection depth of 6–10 nm, missing Ti signals can be attributed to the presence of biofilm and, therefore, insufficient decontamination. Analysis of titanium disks without prior biofilm contamination showed moderate reductions in the Ti signal after GPAP, EPAP, CHX, and doxycycline as well as a higher N signal (28.0%) for CHX. While the percentage of C was slightly decreased by US, EPAP, and GPAP, it was increased by CHX, doxycycline, NaOCl, and laser therapy. Traces of Si, which is part of the air-polishing powders, were found after air-polishing treatments (Table 2).

Adequately, on zirconium surfaces with biofilm, GPAP, EPAP, and NaOCl led to increased Zr signals corresponding to increased biofilm reduction compared with control disks and other decontaminations. Zirconium disks without biofilm showed a decreased frequency of Zr after US and CHX treatment. US-treated surfaces also included Fe and Cr, which are components of the stainless steel tips. Yttrium, a part of the elementary composition of all zirconium disks, was found in all biofilm-free samples. The presence of C signal was increased after CHX treatment, whereas all other treatments did not show striking deviations (Table 3).

## 4 | DISCUSSION

Decontamination of implant surfaces is a key factor for the success in the treatment of peri-implant mucositis and peri-implantitis (Daubert & Weinstein, 2019; Koo et al., 2019). Thereby, efficient biofilm reduction from implant surfaces with minimal or no adverse effects of surrounding soft and hard tissues is highly desirable. To the best of our best knowledge, the present study is the first investigating the efficiency of different decontamination methods and their biocompatibility using cell culture and elementary structure analyses on both titanium and zirconium surfaces. Most of the previous in vitro studies on biofilm reduction in implant surfaces used mono- (Batalha et al., 2021; Ichioka et al., 2021) or multispecies biofilms (Cordeiro et al., 2021; Eick

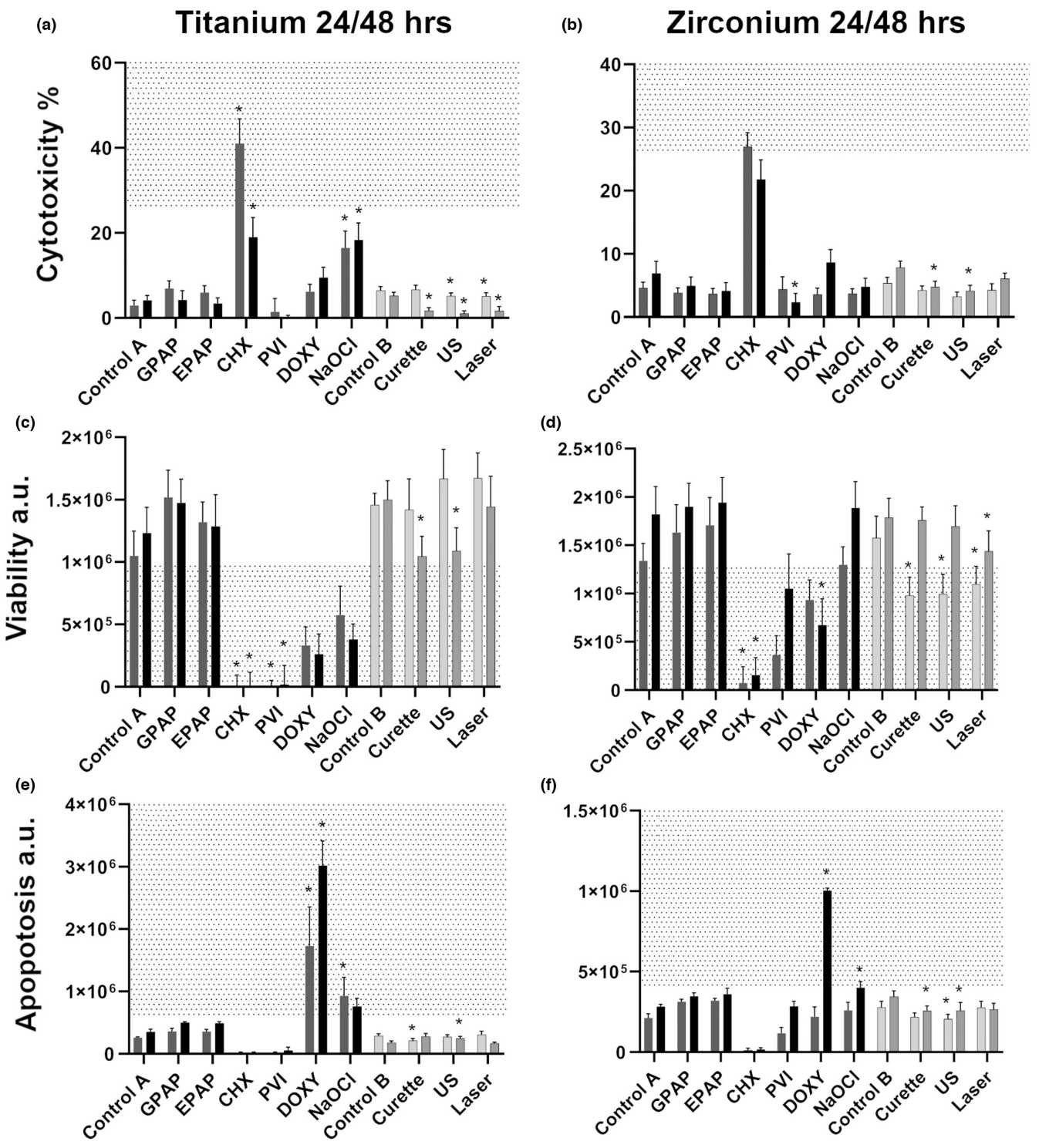


**FIGURE 2** Cytocompatibility of decontamination methods on zirconium and titanium samples as combination of three independent test kits for cytotoxicity (a and b), cell viability (c and d), and apoptosis (e and f) analyzing three different parameters from one single sample, consecutively. Experiments were divided into two separate approaches including the representative controls a and b (untreated samples) shown in different shades of gray. Measurements were done using an immortalized hGF cell line. Results are displayed as means with representative standard deviation based on triplet measurement for 24 h (left bar) and 48 h (right bar). Statistically significant differences ($p < .05$) of the treatment method compared with the untreated control are marked with asterisks. The dotted area illustrates a range that deviates more than 25% from the controls. Values within this range are considered as relevantly increased or decreased values.

et al., 2017; Leung et al., 2022), which might not meet the complexity of peri-implant biofilms in patients with peri-implant inflammatory diseases (Padial-Molina et al., 2016; Rakic et al., 2016). Therefore, a new and robust high-adherence biofilm comprising species with high aggregation, adhesion, and net-forming characteristics (Figure S1b,c) was established.

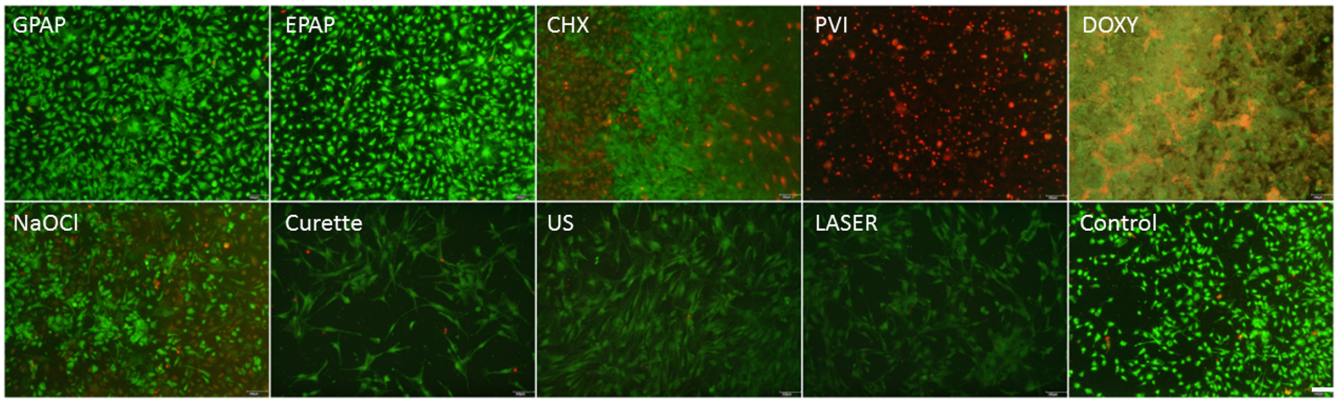


**FIGURE 3** Live/dead staining of gingival fibroblasts 24 h seeded on titanium samples for identification of cytotoxic effects of different mechanical and chemical decontamination pre-treatments. Cytocompatibility can be detected using a live/dead staining with calcein AM and BOBO-3-iodide. This staining results in green, fluorescent viable cells, and red-fluorescent dead cells. Mechanical treatments including powder air-abrasive devices are clearly cytocompatible since all adherent cells are viable (Curette, US, LASER, EPAP, GPAP). PVI treatment results in exclusively dead cells. After CHX, doxy, and NaOCl treatment both, viable and dead cells are present. Microscope objective ×10. Scale bar = 100 µm.

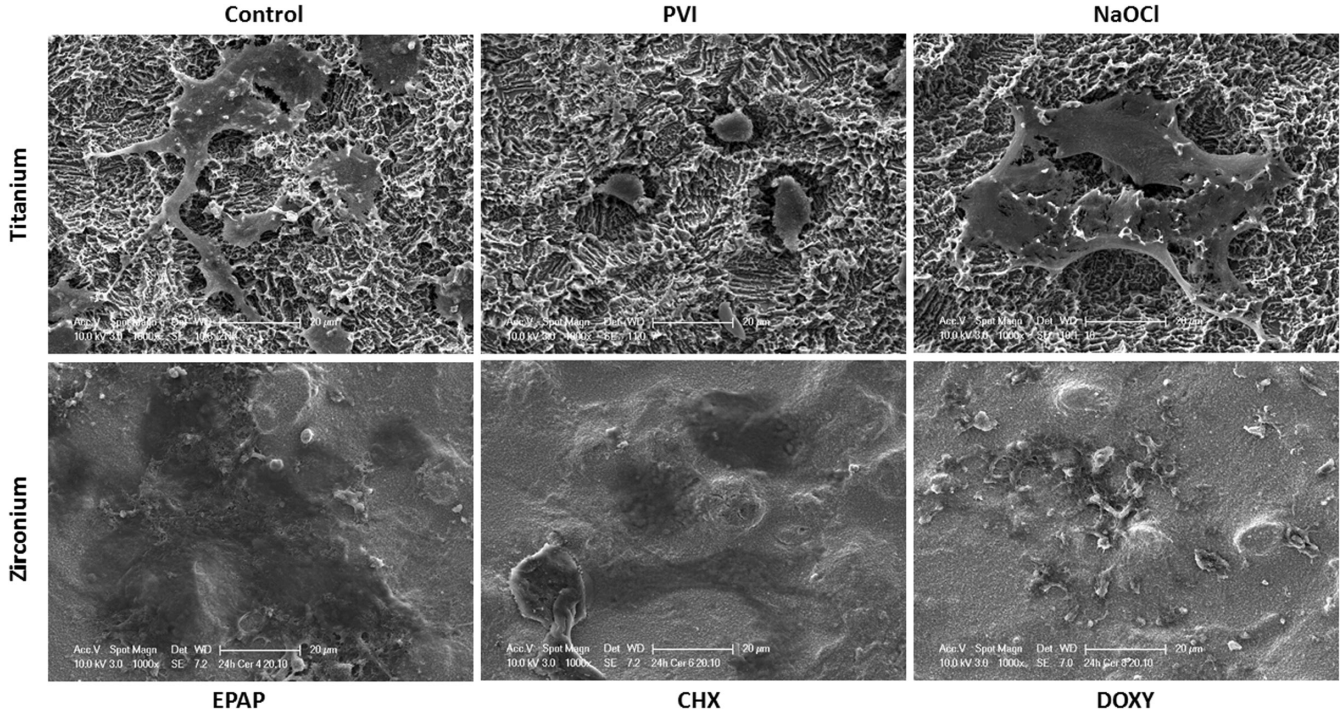


**FIGURE 4** Selection of characteristic SEM images of gingival fibroblasts on titanium (top row) and zirconium (bottom row) specimens. Titanium shows a rough and fissured material surface; the zirconium surface appears amorphous. On titanium, the cells stand out clearly from the background, while on zirconium, the cells appear less clear and shadowlike. Healthy cells (Control, EPAP) show the typical flat fibroblast-like morphology with cell protrusions and filopodia. After PVI treatment, cells are spherical and only loosely attached to the surface. Also, after doxycycline treatment, only cell remnants are visible (doxy). NaOCl and CHX treatment led to mixed cell morphologies of impaired cells. All images at ×1000, scale bar = 20 µm.

Microbiologic data show that US, GPAP, and EPAP treatment led to quantitative biofilm reduction (genome count) on zirconium implants; however, on titanium, no significant changes were found. The latter may reflect the high stability of the presented biofilm model and points to promising benefits of the aforementioned methods on zirconium implants. It may also point to the fact that zirconium allows weaker biofilm adhesion than titanium (do Nascimento et al., 2016; Mathew et al., 2020; Roehling et al., 2017) which, therefore, may facilitate the mechanical biofilm removal on zirconium surfaces. Significant reduction in bacterial activity (rRNA count) was observed for US, GPAP, EPAP, and Er:YAG laser on both titanium and zirconium surfaces. Thus, the physicomechanical treatments were

**TABLE 2** XPS analyses on titanium disks

| Decontamination method | Elementary composition (atomic percentage, %) | | | | |
|---|---|---|---|---|---|
| | Ti | N | C | O | Others |
| Control – *biofilm* | 11.7 | 1.2 | 38.3 | 45.1 | P (1.2), Na (1.7), Ca (0.8) |
| Control + *biofilm* | 0 | 15.4 | 66.5 | 18.1 | |
| Curette – *biofilm* | 9.1 | 3.6 | 39.3 | 46.1 | Na (1.9) |
| Curette + *biofilm* | 0.2 | 10.7 | 67.1 | 22.0 | |
| US – *biofilm* | 16.3 | 1.8 | 25.3 | 56.1 | Ca (0.5) |
| US + *biofilm* | 8.3 | 3.8 | 52.9 | 34.5 | Na (0.5) |
| Laser – *biofilm* | 9.0 | 2.7 | 43.9 | 44.4 | |
| Laser + *biofilm* | 0 | 14.5 | 64.1 | 21.4 | |
| GPAP – *biofilm* | 8.1 | 9.5 | 33.7 | 42.8 | Na (1.2), Si (4.7) |
| GPAP + *biofilm* | 3.4 | 3.3 | 58.8 | 29.0 | Si (5.5) |
| EPAP – *biofilm* | 5.6 | 2.5 | 29.9 | 47.6 | Si (14.4) |
| EPAP + *biofilm* | 2.8 | 4.9 | 64.2 | 19.4 | Si (0.4) |
| CHX – *biofilm* | 8.1 | 28.0 | 45.1 | 42.5 | Na (1.6) |
| CHX + *biofilm* | 0 | 13.5 | 62.0 | 24.1 | |
| Doxy – *biofilm* | 8.1 | 1.2 | 53.3 | 35.2 | Si (2.2) |
| Doxy + *biofilm* | 0.3 | 12.8 | 63.9 | 23.0 | |
| PVI – *biofilm* | 14.0 | 1.3 | 39.8 | 42.7 | Na (1.7), Ca (0.5) |
| PVI + *biofilm* | 0 | 15.5 | 64.0 | 20.3 | I (0.2) |
| NaOCl – *biofilm* | 10.7 | 0 | 45.5 | 41.4 | Na (1.5), Ca (0.9) |
| NaOCl + *biofilm* | 0 | 13.7 | 63.5 | 21.3 | Cl (1.5) |

**TABLE 3** XPS analyses on zirconium disks

| Decontamination method | Elementary composition (atomic percentage) | | | | |
|---|---|---|---|---|---|
| | Zr | N | C | O | Others |
| Control – *biofilm* | 12.9 | 0 | 23 | 54 | Y (1.8), P (2.7), Na (5.6) |
| Control + *biofilm* | 0 | 15.1 | 65.7 | 19.2 | |
| Curette – *biofilm* | 13.5 | 0 | 22.5 | 57.1 | Y (2.1) |
| Curette + *biofilm* | 0.2 | 8.5 | 70.2 | 22.0 | |
| US – *biofilm* | 7.0 | 0 | 34.6 | 48.3 | Y (0.9), Cr (2.4), Na (1.6), Fe (5.2) |
| US + *biofilm* | 0.2 | 0 | 82 | 17.8 | |
| Laser – *biofilm* | 18.0 | 0 | 29.1 | 50.3 | Y (2.6) |
| Laser + *biofilm* | 0.8 | 11.9 | 65.3 | 21.4 | |
| GPAP – *biofilm* | 12.1 | 3.8 | 33.0 | 48.3 | Y (1.9), Na (0.9) |
| GPAP + *biofilm* | 5.6 | 0 | 61.6 | 28.3 | Si (4.5) |
| EPAP – *biofilm* | 17.5 | 5.1 | 24.6 | 49.3 | Y (2.4), Na (1.1) |
| EPAP + *biofilm* | 5.8 | 0 | 67.0 | 27.2 | |
| CHX – *biofilm* | 7.0 | 0.9 | 55.2 | 35.8 | Y (1.1) |
| CHX + *biofilm* | 0.7 | 14.1 | 64.2 | 21.0 | |
| Doxy - *biofilm* | 18.1 | 0 | 27.2 | 51.7 | Y (3.0) |
| Doxy + *biofilm* | 0.8 | 15.4 | 62.6 | 21.2 | |
| PVI – *biofilm* | 19.6 | 0 | 29.0 | 48.4 | Y (3.0) |
| PVI + *biofilm* | 0.9 | 13.1 | 61.9 | 24.0 | I (0.1) |
| NaOCl – *biofilm* | 18.0 | 0 | 29.3 | 50.0 | Y (2.7) |
| NaOCl + *biofilm* | 7.0 | 9.5 | 49.0 | 31.8 | Y (0.9), Na (0.9) |

effective as they disintegrated the biofilm best but not entirely, as 1 (EPAP) – 10% (Er:YAG laser, US) remained (Figure 1a,b). The remaining biofilm was further and considerably affected in activity. The ionic strength of glycine and erythritol, as well as the light and heat of the laser—all water-reducing, drying processes—reduced bacterial activity, even more than with chemical agents/antibiotics. Superior decontamination effects are known for GPAP and EPAP on titanium implants (Mensi et al., 2020) and on zirconium surface for GPAP (John et al., 2016). Thereby, Mensi et al. (2020) noted that in a simulated peri-implant pocket model, a longer treatment time (45 instead of 5 s) even more improved biofilm removal. Pham et al. (2021) demonstrated at zirconium surfaces that both ultrasonic and Er:YAG laser proved better in biofilm reduction than manual instruments, while Eick et al. (2017) and AlMoharib et al. (2021) reported favorable biofilm reduction for Er:YAG on titanium surfaces. Interestingly, out of the chemical decontaminations, only NaOCl showed a significantly higher rRNA count reduction at titanium disks, which is in accordance with previous reports demonstrating effective disinfection by NaOCl in multispecies biofilms on titanium in vitro (Homayouni et al., 2019) and in vivo (Gosau et al., 2010). All other therapies did not provide any significant improvements. The very low (PVI, doxycycline) or missing (CHX) decontamination effects on rRNA count at both materials might be caused by the stability of the established biofilm with a strong diffusion barrier created. This points to the meaning of chemical agents as adjunctive to mechanical decontamination rather than sole therapy. For CHX, which provided least efficiency in our study, a weak antimicrobial effect on single- and multispecies biofilms has already been shown in other studies (Kotsakis et al., 2016; Widodo et al., 2016), while for PVI and doxycycline, only limited data about antibacterial effects are available (Barrak et al., 2020; Bernardi et al., 2019).

Cell culture analyses resulted in low cytotoxicity and apoptosis and high viability for fibroblasts after mechanical treatments (curette and US), GPAP, EPAP, and Er:YAG laser. Even if there was a reduced viability after mechanical and laser treatment on zirconium compared with control disks, this observation should not be considered clinically relevant since it could not be confirmed by the live/dead staining and the SEM images. By contrast, chemotherapeutic agents caused defined effects in cell culture experiments. CHX had the highest cytotoxic effect, which was even more pronounced on titanium and seemed partly reversible after 48 h. This observation is supported by other studies showing a cytotoxic effect of CHX on fibroblasts and osteoblasts (Kotsakis et al., 2016; Rajabalian et al., 2009). Thereby, an effective adsorption of CHX on titanium and zirconium surfaces and a high substantivity might explain its persistently high cytotoxic effect, which has already been demonstrated for titanium implants (Kozlovsky et al., 2006; Ryu et al., 2015). Also, PVI showed a detrimental effect on fibroblasts. Obviously, it caused a prompt dead of the cells, so that LDH secretion (cytotoxicity) and caspase 3/7 activity (apoptosis) were prevented. Also, live/dead staining revealed almost 100% dead cells after 24 h. This confirms that the cells were directly affected, and that absorbance measurement was not disturbed by the PVI color. Cytotoxic effects of povidone-iodine on gingival fibroblasts have been reported by other studies (Barnhart et al., 2005). Beside the moderate cytotoxic potential of NaOCl on titanium-seeded cells, the increasingly high apoptosis values of doxycycline on titanium and zirconium have not been reported. However, since the apoptotic effect of doxycycline is known from tumor cells (Alexander-Savino et al., 2016), it should be verified in future studies and, at least, be carefully considered when slow-release drug devices are applied in dental applications.

In general, the effects of the chemical decontaminations were more pronounced on titanium specimens than on zirconium. This might be based on the higher roughness of the etched titanium surfaces (Figure 4), on which the drugs adhere better and retain longer than on smooth and hydrophobic ceramic surfaces.

Elementary analysis using XPS was performed in a setting with and without prior biofilm contamination. This allowed us to verify and extend microbiologic evaluation of biofilm reduction (with prior contamination) and alterations of elements on the implant surfaces (without prior contamination). On contaminated titanium disks, decontamination with US, GPAP, and EPAP partly re-exposed titanium surfaces (positive titanium signals), while on contaminated zirconium, GPAP, EPAP, and NaOCl showed elevated zirconium signals compared with untreated control disks. Thus, elementary analysis supported the microbiologic findings regarding an effective biofilm inactivation by GPAP and EPAP on both materials and for US on titanium. Interestingly, XPS pointed to a moderate biofilm reduction in NaOCl on zirconium (but not on titanium) contrasting the microbiologic outcomes. However, the extent of biofilm reduction in NaOCl remains unclear and needs to be further elucidated. Interestingly, the favorable biofilm inactivation by Er:YAG laser was not reflected by the re-exposure of titanium or zirconium in the XPS analysis. Missing re-exposure of implant surfaces (persistence of inactivated, carbonized, or modified biofilm remnants) could hinder re-osseointegration (Kamionka et al., 2022) or soft tissue attachment (Lang et al., 2000). From this point of view, curette, CHX, doxycycline, PVI, and Er:YAG laser might be considered inferior to air-abrasives. XPS analyses on disks without prior contamination revealed a decrease in carbon after application of US, EPAP, and GPAP. In an in vitro study, Hori et al. (2011) have demonstrated that cell attachment on titanium surfaces was impaired by increasing percentage of carbon. It can be supposed that decontamination of titanium surfaces with US, EPAP, and GPAP might promote osseointegration and/or fibroblast attachment, while CHX, doxycycline, NaOCl, and laser therapy (higher carbon values) might impair cell attachment. On zirconium, these effects might not be presumed since no relevant carbon changes were observed.

## 5 | CONCLUSIONS AND LIMITATIONS

The results of the present study revealed that mechanical decontamination using GPAP, EPAP, ultrasonic, and Er:YAG laser effectively inactivated a very robust high-adherence biofilm without any effect on cytocompatibility and without relevant differences between

titanium and zirconium surfaces. However, only air-abrasives and ultrasonic led to a relevant re-exposure of implant surfaces and, therefore, might promote cell re-attachment. By contrast, chemical agents had no (doxycycline, CHX, and PVI) or only limited (NaOCl) antimicrobial effect with impaired cytocompatibility. Thus, considering characteristics of most effective biofilm modulation and lowest impairment of biocompatibility, data of the present study support the recommendation of ultrasonics and air-abrasives for both titanium and zirconium implant surfaces.

There are a few limitations and practical implications that should be considered. First, it should be noted that in the cell culture test agents were not inactivated by rinsing. In a pre-test series of this study, the same cell culture experiments have been performed with subsequent rinsing of the decontaminated disks after an exposure time of 2 min using 6x1-ml NaCl. In these tests, no significant changes were found regarding cytotoxicity, viability, and apoptosis (data not shown). Thus, the presented unfavorable cell responses by CHX, PVI, and doxycycline may only be expected when inactivation by subsequent rinsing is not performed. During non-surgical treatments, clearance of the sulcus fluid will inactivate the applied agent shortly (Oosterwaal et al., 1990), whereas in surgical situations, agents should be removed after a limited exposure time by careful rinsing. Second, in the present study, combinations of mechanical and chemical decontaminations were not investigated. However, while mechanical or physical decontamination aim to disrupt the biofilm, adjunctive application of chemical agents (such as PVI or doxycycline) might support its inactivation in areas of residual biofilm remnants. Thus, combined approaches might be more beneficial (Büchter et al., 2004; Stein et al., 2017) compared with mechanical means only. Finally, the present study did not consider the macrostructure of implants, which limits efficiency of ultrasonic and curettes. In implant pocket models, previous studies showed disadvantages of curettes and ultrasonic compared with air-abrasives (Keim et al., 2019; Sahrmann et al., 2015) since instrumentation between implant threads was inferior. Therefore, the here presented positive effects of ultrasonic and laser therapy may not or only partly be achieved in vivo dependent on the accessibility of the implants.

## AUTHOR CONTRIBUTIONS

Jamal M. Stein and Sareh Said Yekta-Michael conceived the idea. Georg Conrads and Mohamed M. H. Abdelbary established the high-adherence biofilm and conducted microbiologic analyses. Jamal M. Stein, Sareh Said Yekta-Michael, and Gelareh Sadvandi performed decontamination procedures. Patricia Buttler, Joanna Glock, and Gelareh Sadvandi carried out cell culture experiments. Robert Kaufmann performed XPS analyses. Jamal M. Stein, Mohamed M. H. Abdelbary, Joanna Glock, and Christian Apel analyzed data. Jamal M. Stein, Georg Conrads, and Christian Apel led the writing. Jamal M. Stein and Christian Apel managed and coordinated the group.

## ACKNOWLEDGMENTS

The authors would like to thank the Oral Reconstruction Foundation for the research grant (ORF11802) and the material support. The authors would specially thank Mr. Stephan Rütten for his appreciated support in the performance and analyses of SEM images.

## FUNDING INFORMATION

This study was funded by a grant from the Oral Reconstruction Foundation (Basel, Switzerland).

## CONFLICT OF INTEREST

All authors declare no conflicts of interest related to this study.

## DATA AVAILABILITY STATEMENT

The data that support the findings of this study are available from the corresponding author upon reasonable request.

## ORCID

*Jamal M. Stein* https://orcid.org/0000-0002-7058-1555
*Georg Conrads* https://orcid.org/0000-0003-2577-5294

## REFERENCES

Alexander-Savino, C. V., Hayden, M. S., Richardson, C., Zhao, J., & Poligone, B. (2016). Doxycycline is an NF-κB inhibitor that induces apoptotic cell death in malignant T-cells. *Oncotarget*, *7*, 75954–75967.

AlMoharib, H. S., Steffensen, B., Zoukhri, D., Finkelman, M., & Gyurko, R. (2021). Efficacy of an Er:YAG laser in the decontamination of dental implant surfaces: An in vitro study. *Journal of Periodontology*, *92*, 1613–1621.

Barnhart, B. D., Chuang, A., Lucca, J. J., Roberts, S., Liewehr, F., & Joyce, A. P. (2005). An in vitro evaluation of the cytotoxicity of various endodontic irrigants on human gingival fibroblasts. *Journal of Endodontics*, *31*, 613–615.

Barrak, I., Baráth, Z., Tián, T., Venkei, A., Gajdács, M., Urbán, E., & Stájer, A. (2020). Effects of different decontaminating solutions used for the treatment of peri-implantitis on the growth of Porphyromonas gingivalis-an in vitro study. *Acta Microbiological et Immunologica Hungaria*, *68*, 40–47.

Batalha, V. C., Bueno, R. A., Fronchetti Junior, E., Mariano, J. R., Santin, G. C., Freitas, K. M. S., Ortiz, M. A. L., & Salmeron, S. (2021). Dental implants surface in vitro decontamination protocols. *European Journal of Dentistry*, *15*, 407–411.

Becker, J., John, G., Becker, K., Mainusch, S., Diedrichs, G., & Schwarz, F. (2017). Clinical performance of two-piece zirconia implants in the posterior mandible and maxilla: a prospective cohort study over 2 years. *Clinical Oral Implants Research*, *28*, 29–35.

Bernardi, S., Bianchi, S., Tomei, A. R., Continenza, M. A., & Macchiarelli, G. (2019). Microbiological and SEM-EDS evaluation of titanium surfaces exposed to periodontal gel: In vitro study. *Materials (Basel)*, *12*, 1448.

Büchter, A., Meyer, U., Kruse-Lösler, B., Joos, U., & Kleinheinz, J. (2004). Sustained release of doxycycline for the treatment of peri-implantitis: randomised controlled trial. *British Journal of Oral and Maxillofacial Surgery*, *42*, 439–444.

Chan, H. L., Lin, G. H., Suarez, F., MacEachern, M., & Wang, H. L. (2014). Surgical management of peri-implantitis: a systematic review and meta-analysis of treatment outcomes. *Journal of Periodontology*, *85*, 1027–1041.

Charalampakis, G., & Belibasakis, G. N. (2015). Microbiome of peri-implant infections: lessons from conventional, molecular and metagenomic analyses. *Virulence*, *6*, 183–187.

Chen, Y., Shi, T., Li, Y., Huang, L., & Yin, D. (2022). *Fusobacterium nucleatum*: The opportunistic pathogen of periodontal and peri-implant diseases. *Frontiers in Microbiology*, *13*, 860149.

Comisso, I., Arias-Herrera, S., & Gupta, S. (2021). Zirconium dioxide implants as an alternative to titanium: A systematic review. *Journal of Clinical and Experimental Dentistry*, *13*, e511–e519.

Cordeiro, J. M., Pires, J. M., Souza, J. G. S., Lima, C. V., Bertolini, M. M., Rangel, E. C., & Barão, V. A. R. (2021). Optimizing citric acid protocol to control implant-related infections: An in vitro and in situ study. *Journal of Periodontal Research*, *56*, 558–568.

Daubert, D. M., & Weinstein, B. F. (2019). Biofilm as a risk factor in implant treatment. *Periodontology, 2000*(81), 29–40.

D'Ercole, S., Cellini, L., Pilato, S., Di Lodovico, S., Iezzi, G., Piattelli, A., & Petrini, M. (2020). Material characterization and *Streptococcus oralis* adhesion on Polyetheretherketone (PEEK) and titanium surfaces used in implantology. *Journal of Materials Science: Materials in Medicine*, *31*, 84.

do Nascimento, C., Pita, M. S., de Souza Santos, E., Monesi, N., Pedrazzi, V., Albuquerque Junior, R. F., & Ribeiro, R. F. (2016). Microbiome of titanium and zirconia dental implants abutments. *Dental Materials*, *32*, 93–101.

Dostie, S., Alkadi, L. T., Owen, G., Bi, J., Shen, Y., Haapasalo, M., & Larjava, H. S. (2017). Chemotherapeutic decontamination of dental implants colonized by mature multispecies oral biofilm. *Journal of Clinical Periodontology*, *44*, 403–409.

Eick, S., Meier, I., Spoerlé, F., Bender, P., Aoki, A., Izumi, Y., Salvi, G. E., & Sculean, A. (2017). In vitro-activity of Er:YAG laser in comparison with other treatment modalities on biofilm ablation from implant and tooth surfaces. *PLoS One*, *12*, e0171086.

Faggion, C. M., Jr., Listl, S., Frühauf, N., Chang, H. J., & Tu, Y. K. (2014). A systematic review and Bayesian network meta-analysis of randomized clinical trials on non-surgical treatments for peri-implantitis. *Journal of Clinical Periodontology*, *41*, 1015–1025.

Fretwurst, T., Müller, J., Larsson, L., Bronsert, P., Hazard, D., Castilho, R. M., Kohal, R., Nelson, K., & Iglhaut, G. (2021). Immunohistological composition of peri-implantitis affected tissue around ceramic implants-A pilot study. *Journal of Periodontology*, *92*, 571–579.

Gosau, M., Hahnel, S., Schwarz, F., Gerlach, T., Reichert, T. E., & Bürgers, R. (2010). Effect of six different peri-implantitis disinfection methods on in vivo human oral biofilm. *Clinical Oral Implants Research*, *21*, 866–872.

Hauser-Gerspach, I., Kulik, E. M., Weiger, R., Decker, E. M., Von Ohle, C., & Meyer, J. (2007). Adhesion of *Streptococcus sanguinis* to dental implant and restorative materials in vitro. *Dental Materials Journal*, *26*, 361–366.

Heitz-Mayfield, L. J. A., & Salvi, G. E. (2018). Peri-implant mucositis. *Journal of Periodontology*, *89*, 257–266.

Henne, K., Gunesch, A. P., Walther, C., Meyer-Lueckel, H., Conrads, G., & Esteves-Oliveira, M. (2016). Analysis of bacterial activity in sound and cariogenic biofilm: A pilot in vivo study. *Caries Research*, *50*, 480–488.

Homayouni, A., Bahador, A., Moharrami, M., Pourhajibagher, M., Rasouli-Ghahroudi, A. A., & Alikhasi, M. (2019). Effect of 5 popular disinfection methods on microflora of laboratory: Customized implant abutments. *Implant Dentistry*, *28*, 437–446.

Hori, N., Iwasa, F., Tsukimura, N., Sugita, Y., Ueno, T., Kojima, N., & Ogawa, T. (2011). Effects of UV photofunctionalization on the nanotopography enhanced initial bioactivity of titanium. *Acta Biomaterialia*, *7*, 3679–3691.

Ichioka, Y., Derks, J., Dahlén, G., Berglundh, T., & Larsson, L. (2021). In vitro evaluation of chemical decontamination of titanium discs. *Scientific Reports*, *11*, 22753.

John, G., Becker, J., & Schwarz, F. (2016). Effectivity of air-abrasive powder based on glycine and tricalcium phosphate in removal of initial biofilm on titanium and zirconium oxide surfaces in an ex vivo model. *Clinical Oral Investigation*, *20*, 711–719.

Kamionka, J., Matthes, R., Holtfreter, B., Pink, C., Schlüter, R., von Woedtke, T., Kocher, T., & Jablonowski, L. (2022). Efficiency of cold atmospheric plasma, cleaning powders and their combination for biofilm removal on two different titanium implant surfaces. *Clinical Oral Investigations*, *26*, 3179–3187. https://doi.org/10.1007/s00784-021-04300-0. Online ahead of print.

Keim, D., Nickles, K., Dannewitz, B., Ratka, C., Eickholz, P., & Petsos, H. (2019). In vitro efficacy of three different implant surface decontamination methods in three different defect configurations. *Clinical Oral Implants Research*, *30*, 550–558.

Koo, K. T., Khoury, F., Keeve, P. L., Schwarz, F., Ramanauskaite, A., Sculean, A., & Romanos, G. (2019). Implant surface decontamination by surgical treatment of periimplantitis: A literature review. *Implant Dentistry*, *28*, 173–176.

Kotsakis, G. A., Lan, C., Barbosa, J., Lill, K., Chen, R., Rudney, J., & Aparicio, C. (2016). Antimicrobial agents used in the treatment of peri-implantitis alter the physicochemistry and cytocompatibility of titanium surfaces. *Journal of Periodontololgy*, *87*, 809–819.

Kozlovsky, A., Artzi, Z., Moses, O., Kamin-Belsky, N., & Greenstein, R. B. (2006). Interaction of chlorhexidine with smooth and rough types of titanium surfaces. *Journal of Periodontology*, *77*, 1194–1200.

Lang, N. P., Wilson, T. G., & Corbet, E. F. (2000). Biological complications with dental implants: their prevention, diagnosis and treatment. *Clinical Oral Implants Research*, *11*, 146–155.

Leung, K., Bi, J., Giannelis, G., Owen, G., & Larjava, H. (2022). Decontamination of multispecies oral biofilm from rough implant surface by airflow with glycine. *Clinical and Experimental Dental Research*, *8*(1), 322–328.

Mathew, M. G., Samuel, S. R., Soni, A. J., & Roopa, K. B. (2020). Evaluation of adhesion of *Streptococcus mutans*, plaque accumulation on zirconia and stainless steel crowns, and surrounding gingival inflammation in primary molars: randomized controlled trial. *Clinical Oral Investigation*, *24*, 3275–3280.

Mensi, M., Viviani, L., Agosti, R., Scotti, E., Garzetti, G., & Calza, S. (2020). Comparison between four different implant surface debridement methods: an in-vitro experimental study. *Minerva Stomatologica*, *69*, 286–294.

Nadkarni, M. A., Martin, F. E., Jacques, N. A., & Hunter, N. (2002). Determination of bacterial load by real-time PCR using a broad-range (universal) probe and primers set. *Microbiology*, *148*, 257–266.

Oosterwaal, P. J., Mikx, F. H., & Renggli, H. H. (1990). Clearance of a topically applied fluorescein gel from periodontal pockets. *Journal of Clinical Periodontology*, *17*, 613–615.

Padial-Molina, M., López-Martínez, J., O'Valle, F., & Galindo-Moreno, P. (2016). Microbial profiles and detection techniques in peri-implant diseases: A systematic review. *Journal of Oral Maxillofacial Research*, *7*, e10.

Pham, C. M., Chen, C. Y., & Kim, D. M. (2021). The effects of using erbium, chromium-doped:yttrium-scandium-gallium-garnet laser on the surface modification, bacterial decontamination, and cell adhesion on zirconia discs: an in vitro study. *Lasers in Medica Science*, *36*, 1701–1708.

Rajabalian, S., Mohammadi, M., & Mozaffari, B. (2009). Cytotoxicity evaluation of Persica mouthwash on cultured human and mouse cell lines in the presence and absence of fetal calf serum. *Indian Journal of Dental Research*, *20*, 169–173.

Rakic, M., Grusovin, M. G., & Canullo, L. (2016). The microbiologic profile associated with peri-implantitis in humans: A systematic review. *International Journal of Oral & Maxillofacial Implants*, *31*, 359–368.

Renvert, S., Persson, G. R., Pirih, F. Q., & Camargo, P. M. (2018). Peri-implant health, peri-implant mucositis, and peri-implantitis: Case definitions and diagnostic considerations. *Journal of Periodontology*, *89*, 304–312.

Roehling, S., Astasov-Frauenhoffer, M., Hauser-Gerspach, I., Braissant, O., Woelfler, H., Waltimo, T., Kniha, H., & Gahlert, M. (2017). In vitro biofilm formation on titanium and zirconia implant surfaces. *Journal of Periodontology*, *88*, 298–307.

Ryu, H. S., Kim, Y. I., Lim, B. S., Lim, Y. J., & Ahn, S. J. (2015). Chlorhexidine uptake and release from modified titanium surfaces and its antimicrobial activity. *Journal of Periodontology*, *86*, 1268–1275.

Sahrmann, P., Ronay, V., Hofer, D., Attin, T., Jung, R. E., & Schmidlin, P. R. (2015). In vitro cleaning potential of three different implant debridement methods. *Clinical Oral Implants Research*, *26*, 314–319.

Sanz-Martín, I., Paeng, K., Park, H., Cha, J. K., Jung, U. W., & Sanz, M. (2021). Significance of implant design on the efficacy of different peri-implantitis decontamination protocols. *Clinical Oral Investigations*, *25*, 3589–3597.

Schwarz, F., Schmucker, A., & Becker, J. (2015). Efficacy of alternative or adjunctive measures to conventional treatment of peri-implant mucositis and peri-implantitis: a systematic review and meta-analysis. *International Journal of Implant Dentistry*, *1*, 22.

Steiger-Ronay, V., Merlini, A., Wiedemeier, D. B., Schmidlin, P. R., Attin, T., & Sahrmann, P. (2017). Location of unaccessible implant surface areas during debridement in simulated peri-implantitis therapy. *BMC Oral Health*, *17*, 137.

Stein, J. M., Hammächer, C., & Said-Yekta Michael, S. (2017). Combination of ultrasonic decontamination, soft tissue curettage and submucosal air polishing with povidone-iodine application for non-surgical therapy of peri-implantitis: 12 months clinical outcomes. *Journal of Periodontology*, *15*, 1–13.

Tuchscheerer, V., Eickholz, P., Dannewitz, B., Ratka, C., Zuhr, O., & Petsos, H. (2021). In vitro surgical and non-surgical air-polishing efficacy for implant surface decontamination in three different defect configurations. *Clinical Oral Investigation*, *25*, 1743–1754.

Ungvári, K., Pelsöczi, I. K., Kormos, B., Oszkó, A., Rakonczay, Z., Kemény, L., Radnai, M., Nagy, K., Fazekas, A., & Turzó, K. (2010). Effects on titanium implant surfaces of chemical agents used for the treatment of peri-implantitis. *Journal of Biomedical Materials Research Part B*, *94*, 222–229.

Walther, C., Zumbülte, S., Faerber, C. M., Wierichs, R. J., Meyer-Lueckel, H., Conrads, G., Henne, K., & Esteves-Oliveira, M. (2021). Analysis of relative bacterial activity and lactate dehydrogenase gene expression of caries-associated bacteria in a site-specific natural biofilm: an ex vivo study. *Clinical Oral Investigation*, *25*, 3669–3679.

Wheelis, S. E., Gindri, I. M., Valderrama, P., Wilson, T. G., Jr., Huang, J., & Rodrigues, D. C. (2016). Effects of decontamination solutions on the surface of titanium: investigation of surface morphology, composition, and roughness. *Clinical Oral Implants Research*, *27*, 329–340.

Widodo, A., Spratt, D., Sousa, V., Petrie, A., & Donos, N. (2016). An in vitro study on disinfection of titanium surfaces. *Clinical Oral Implants Research*, *27*, 1227–1232.

## SUPPORTING INFORMATION

Additional supporting information can be found online in the Supporting Information section at the end of this article.

**How to cite this article:** Stein, J. M., Conrads, G., Abdelbary, M. M. H., Yekta-Michael, S. S., Buttler, P., Glock, J., Sadvandi, G., Kaufmann, R., & Apel, C. (2022). Antimicrobial efficiency and cytocompatibility of different decontamination methods on titanium and zirconium surfaces. *Clinical Oral Implants Research*, *00*, 1–13. https://doi.org/10.1111/clr.14014